Experimental simulation of evaporation-driven silica sinter formation and microbial silicification in hot spring systems.

François Orange, Stefan Lalonde, Kurt O Konhauser

ASTROBIOLOGY
Volume 13, Number 2, 2013

DOI: 10.1089/ast.2012.0887

Experimental Simulation of Evaporation-Driven Silica Sinter Formation and Microbial Silicification in Hot Spring Systems

François Orange,[1,*] Stefan V. Lalonde,[2] and Kurt O. Konhauser[1]

Abstract

Evaporation of silica-rich geothermal waters is one of the main abiotic drivers of the formation of silica sinters around hot springs. An important role in sinter structural development is also played by the indigenous microbial communities, which are fossilized and eventually encased in the silica matrix. The combination of these two factors results in a wide variety of sinter structures and fabrics. Despite this, no previous experimental fossilization studies have focused on evaporative-driven silica precipitation. We present here the results of several experiments aimed at simulating the formation of sinters through evaporation. Silica solutions at different concentrations were repeatedly allowed to evaporate in both the presence and absence of the cyanobacterium *Synechococcus elongatus*. Without microorganisms, consecutive silica additions led to the formation of well-laminated deposits. By contrast, when microorganisms were present, they acted as reactive surfaces for heterogeneous silica particle nucleation; depending on the initial silica concentration, the deposits were then either porous with a mixture of silicified and unmineralized cells, or they formed a denser structure with a complete entombment of the cells by a thick silica crust. The deposits obtained experimentally showed numerous similarities in terms of their fabric to those previously reported for natural hot springs, demonstrating the complex interplay between abiotic and biotic processes during silica sinter growth. Key Words: Silica—Cyanobacteria—Fossilization—Hot springs—Stromatolites. Astrobiology 13, 163–176.

1. Introduction

Silica sinter deposits that are commonly found around hot springs form as a result of the abiotic precipitation of dissolved silica contained in geothermal waters after they have reached the surface. Water evaporation is, along with cooling, one of the main abiotic drivers of precipitation and consequently of sinter formation (Walter, 1972, 1976a, 1976b; Jones *et al.,* 1998; Braunstein and Lowe, 2001; Mountain *et al.,* 2003; Handley *et al.,* 2005; Schinteie *et al.,* 2007; Tobler *et al.,* 2008). Indeed, *in situ* studies in which sinter growth on glass slides has been examined (Mountain *et al.,* 2003; Handley *et al.,* 2005, 2008; Schinteie *et al.,* 2007; Tobler *et al.,* 2008) have shown that sinter growth occurs mainly above the air-water interface as the result of evaporation of silica-rich water supplied by waves, splashes, or capillary action. Evaporation may also occur rapidly wherever the water level is low and in zones irregularly covered by water, such as around geysers or in irregular or terraced hot spring outflows (Walter, 1972, 1976a; Jones *et al.,* 1998). Generally speaking, subaerial sinter formation depends on the spring style and activity (*i.e.,* quiet, surging, boiling, geyser) and on the frequency of wetting (Braunstein and Lowe, 2001).

In situ studies have also revealed that the microbial communities that thrive around hot springs and their outflows play an important role in the formation of silica sinters. By acting as a reactive substratum for passive and heterogeneous silica nucleation, these microorganisms become very rapidly fossilized and eventually encased in the newly formed sinter (Schultze-Lam *et al.,* 1995; Cady and Farmer, 1996; Renaut *et al.,* 1996; Jones *et al.,* 1997, 1998, 2000, 2001, 2003, 2004, 2008; Konhauser *et al.,* 2001; Mountain *et al.,* 2003; Kyle *et al.,* 2007; Tobler *et al.,* 2008). The structure of the microbial communities, as well as their daily or seasonal growth variations, thus also contribute to the development of the fabrics and structure of their entombing sinters (Walter *et al.,* 1976; Hinman and Lindstrom, 1996; Konhauser *et al.,* 2001, 2004; Jones *et al.,* 2005; Berelson *et al.,* 2011).

[1]Department of Earth and Atmospheric Sciences, University of Alberta, Edmonton, Alberta, Canada.
[2]UMR 6538 Domaines Océaniques, Institut Universitaire Européen de la Mer, Université de Bretagne Occidentale, Technopôle Brest-Iroise, Plouzané, France.
*Present address: University of Puerto Rico, Nanoscopy Facility, Facultad de Ciencias Naturales, Departamento de Fisica, San Juan, Puerto Rico, USA.

Consequently, sinter micro- and macrostructures are determined or influenced by a large number of parameters, which explains the large diversity of facies observed (*e.g.,* Jones *et al.,* 1998; Braunstein and Lowe, 2001; Schinteie *et al.,* 2007) and the difficulties at deciphering the processes involved.

However, very little is understood about the evaporative precipitation process; despite several decades of experimental studies in which the silicification of microbes was examined, only one (Yee *et al.,* 2003) involved examination of silicification after cooling-induced supersaturation. In all other experimental studies, rapid pH neutralization was employed to induce silica deposition (*e.g.,* Ferris *et al.,* 1988; Birnbaum *et al.,* 1989; Westall *et al.,* 1995; Westall, 1997; Phoenix *et al.,* 2000; Toporski *et al.,* 2002; Yee *et al.,* 2003; Benning *et al.,* 2004a, 2004b; Lalonde *et al.,* 2005; Orange *et al.,* 2009, 2013), and evaporation as a viable pathway for rapid cellular fossilization was neither considered nor examined. Accordingly, the rationale for this study was to reproduce, in a simple way, the formation of laminated silica sinter in both the presence and absence of microorganisms and exclusively by evaporative processes. Through experiments involving successive cycles of addition and evaporation of undersaturated and oversaturated silica solutions, the following aspects of evaporation-induced silica deposition were examined: (1) how silica precipitates by evaporation either in the absence or presence of microorganisms, (2) whether successive addition/evaporation cycles can form sinter fabrics or laminations, (3) what role microorganisms have on the deposition of silica or the structure of the deposit, and (4) how evaporative silica deposition relates to sinter formation in natural settings with respect to deposition rate and silica saturation state.

2. Material and Methods

2.1. Cell culturing

The obligate photoautotrophic cyanobacterium *Synechoccoccus elongatus* PCC 7942 was chosen for this study because it is a model organism commonly used in prior cyanobacterial studies (*e.g.,* Chen, 2007), diverse members of this genus inhabit the surface layers of hot spring microbial mats (*e.g.,* Walter *et al.,* 1972; Ferris *et al.,* 1996; Jones *et al.,* 1998), and its rod morphology facilitates identification in microscopy. Cultures were grown in liquid BG-11 media (Rippka *et al.,* 1979) with constant illumination, shaking, and bubbling with filtered and humidified air (Chamot and Owttrim, 2000). Cell pellets were recovered from stationary phase cultures by centrifugation (7500 rpm, 15 min) and stored at 4°C until use.

2.2. Experimental silica mineralization

The goal of this experiment was to mimic hot spring conditions where silica-rich waters become rapidly silica-oversaturated as the result of cooling, evaporation, or pH change (*e.g.,* White *et al.,* 1956; Fournier, 1985; Jones *et al.,* 1998) shortly before or upon contact with microbial mats. We used alkaline monomeric silica solutions at three different concentrations (30, 150, and 300 ppm Si) similar to those encountered in hot spring systems (*e.g.,* Mountain *et al.,* 2003; Tobler *et al.,* 2008). The pH of these solutions was lowered from pH ~11 to ~8 immediately before exposure to *S. elongatus* cell concentrates, thus making the 300 ppm Si and 150 ppm Si silica-oversaturated (amorphous silica solubility at 20°C: 49 ppm Si, calculated from the equilibrium equation of Gunnarsson and Arnórsson, 2000). Oversaturation of the 30 ppm Si solution was only achieved during evaporation. A 300 ppm Si stock solution was prepared by diluting 0.304 g of $Na_2SiO_3 \cdot 9H_2O$ (Fisher Scientific, Nepean, ON) in 100 mL of ultrapure water. Part of this solution was then diluted either 2× or 10× to obtain solutions of 150 ppm Si and 30 ppm Si, respectively.

For each experiment, 20 μL of the cell pellet was spread in a polystyrene weighing dish and left to dry (Fig. 1). One milliliter of silica solution was then added to completely cover the deposited cells. Immediately before addition, the pH of the silica solution was lowered to ~8 with 0.12 or 1.2 *M* HCl. Samples were then left to dry at room temperature. Complete drying usually occurred after ~36 h. The addition of 1 mL of silica solution and its drying is hereafter referred to in this study as "a cycle." The following experiments were conducted: (1) 10 cycles with a 30 ppm Si solution, (2) 10 cycles with a 150 ppm Si solution, (3) 1 cycle with a 300 ppm Si solution [amount of silica equivalent to (1)], (4) 10 cycles with a 300 ppm Si solution, and (5) control samples with no cells and 2 cycles with either 30 or 300 ppm Si silica solutions. With every successive addition and drying of silica solution, a deposit of increasing thickness formed at the bottom of the polystyrene dishes (Fig. 1).

2.3. Scanning electron microscopy

For both samples with cell pellets and for controls, areas of interest were identified by light microscopy, carefully excised as 5×5 mm squares (two per sample), and then delicately rinsed three times in ultrapure water to dissolve NaCl deposited during the final stages of evaporation. Samples were placed on silver-painted scanning electron microscope (SEM) sample stubs and gold coated. SEM observations were performed at 5 kV with a JEOL 6301F field emission gun scanning electron microscope in the Department of Earth and Atmospheric Sciences at the University of Alberta.

3. Results

3.1. Light microscopy

The cell pellets used for these experiments were highly concentrated such that a small volume (20 μL) was sufficient to cover the bottom of the polystyrene dishes with a bright green deposit made of multiple layers of densely packed *S. elongatus* cells (Figs. 1, 3a). Silica addition led, at least in the first cycles, to the partial resuspension of the initial deposited cells or the clumping and detachment of some cell material (small dark aggregates, Fig. 1a, 1b, 1d). The color of the deposited cells became progressively more yellowish with time. The thickness of the silica deposit was directly related to the silica concentration. In the 300 ppm Si experiment, the deposited cell pellets were completely encrusted by silica after 10 cycles (Fig. 1d), with biomass appearing faded under a visible layer of silica that was somewhat frosted in appearance (compare Fig. 1c and 1d). Small, bright NaCl crystals could at times be seen with the naked eye on top of the deposit, especially for the highest Si concentrations (Fig. 1b, 1d, arrows).

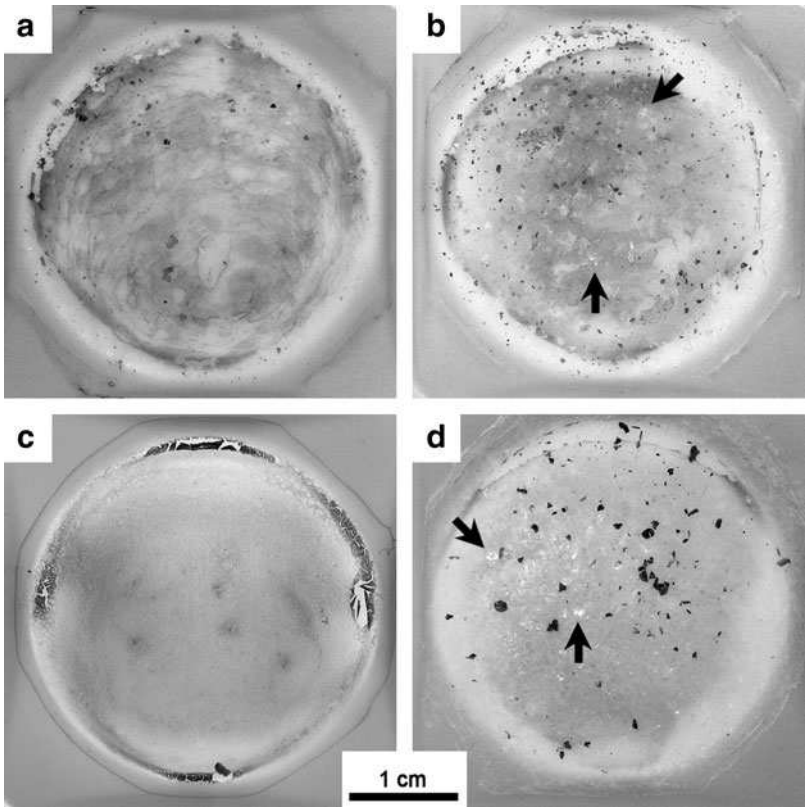

FIG. 1. Images of silica-treated *Synechococcus elongatus* cell pellets at the end of the experiments. (**a**) After 10 addition/drying cycles with 30 ppm Si solution. (**b**) 10 cycles, 150 ppm Si. (**c**) 1 cycle, 300 ppm Si. (**d**) 10 cycles, 300 ppm Si. ~1 mm NaCl crystals (arrows) and clumping or flaking of dark cell-mineral aggregate are apparent in experiments with multiple cycles (a, b, d).

3.2. Scanning electron microscopy

In the inorganic controls, SEM micrographs of the 30 ppm Si sample showed that 2 cycles of silica addition resulted in a layered structure in the deposit that formed at the bottom of the polystyrene dish (Fig. 2a). Two granular layers of silica, corresponding to the two additions of silica solution (*i.e.,* 2 cycles), were visible along with a layer of smooth NaCl precipitate intermittently covering the silica (Fig. 2a). The silica layers were quite homogeneous and composed of 30–40 nm sized silica particles (Fig. 2b, 2c). The NaCl layer apparently formed over deposited silica and likely represents late-stage precipitation during evaporation as the result of concentrating Na^+ (from the sodium silicate solution) and Cl^- ions (from the HCl used for pH adjustment). These ions had similar molar concentrations in the added solution (with a small excess of Na^+) (Table 1). Two cycles of 300 ppm Si solution addition resulted in the formation of a ~3 μm thick deposit (Fig. 2e). Despite the fact that the 300 ppm Si solution was initially supersaturated with respect to amorphous silica, the 300 ppm Si control sample showed features very similar to the 30 ppm Si control sample (with an undersaturated solution). Most of this deposit was formed of granular silica precipitate with sizes similar to the 30 ppm Si control experiment (30–40 nm; Fig. 2f).

In the 300 ppm Si experiments, desiccation cracks formed in the silica mass, both vertically and horizontally, resulting at times in separation of the two layers corresponding to the two silica additions (Fig. 2d, 2e). NaCl deposits again formed on the silica layer but did not cover it completely, and in places it appeared distinctly more crystalline and associated with desiccation features (Fig. 2d). In cross section the top silica layer appeared thinner than the bottom layer (Fig. 2f), suggesting that, after the second addition of saturated silica solution, silica may have penetrated and precipitated within void space of the first silica layer. No traces of NaCl deposit could be seen between the two silica layers (Fig. 2f), suggesting that the NaCl deposit formed at the end of the first cycle was completely dissolved after the second addition of fresh silica solution.

For experiments with cell pellets, repeated silica treatments do not appear to have significantly resuspended the deposited cell mass. After 10 cycles of 30 ppm Si solution, *S. elongatus* cells remained densely packed (Fig. 3a) and appear to have retained smooth extracellular polymeric substance (EPS) covering material (Fig. 3b). The cells showed no evidence of significant deformation or degradation. After 10 cycles with 30 ppm Si solution, silicification was manifested in three different ways: (i) as homogeneous deposits made of 20–50 nm silica particles on the surface of the polystyrene weighing dishes between, and adjacent to, the deposited cell mass (Fig. 3e)—these were similar in size to those observed in control samples (*e.g.,* Fig. 2c); (ii) as larger agglomerates (hundreds of nanometers) composed of 30–70 nm silica particles, deposited on, or intertwined within, the silica-cell mass (larger, brighter particles in Fig. 3b–d); and (iii) as coatings directly on cell or EPS surfaces where the silica is clearly more fine-grained than in the case of (ii) (30–50 nm), yet it retains a granular appearance (exemplified by cells directly center of Fig. 3c). No layering of the silica precipitate was observed in the 30 ppm Si cell pellet experiments. The dense mass of cells, providing a template for the deposition of silica, apparently prevented the formation of distinct layers at scales commensurate with a single cycle of silica

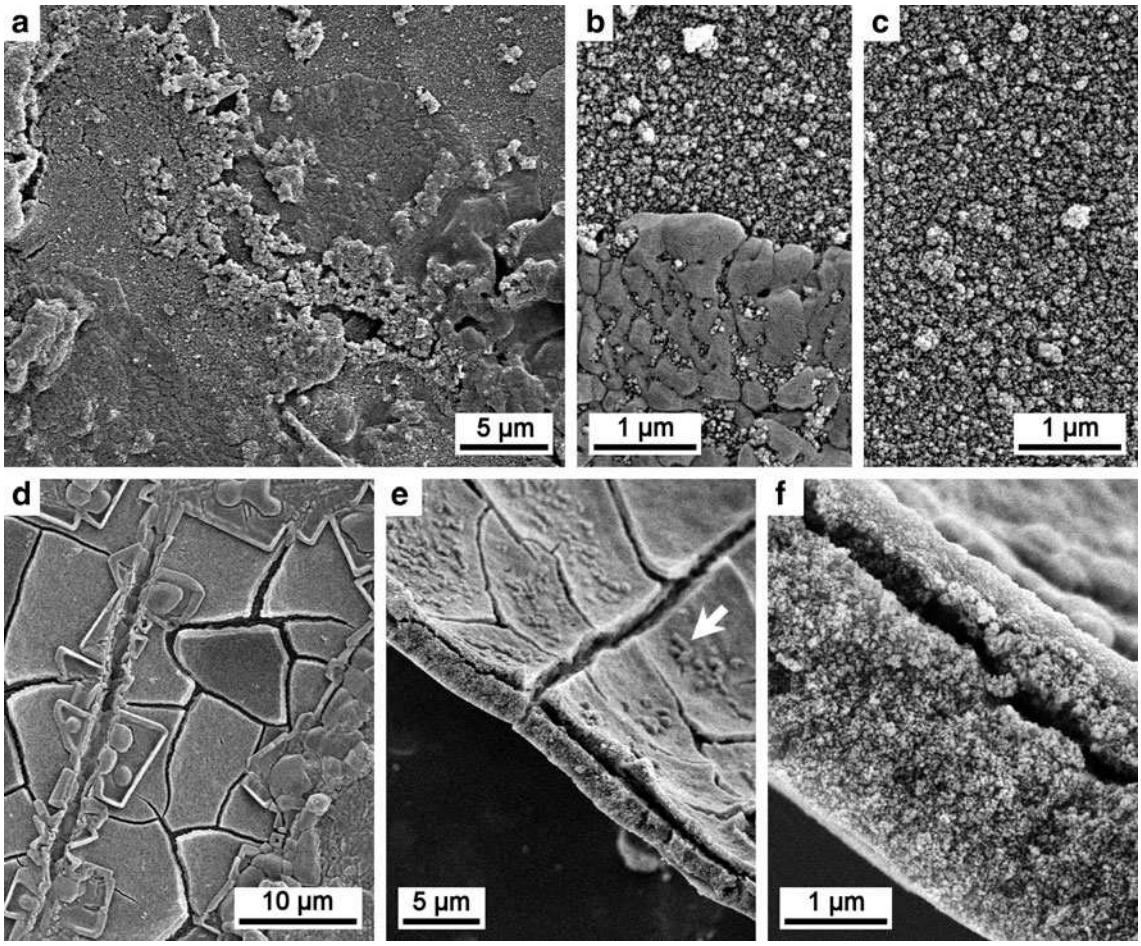

FIG. 2. SEM micrographs showing precipitates formed in control experiments (no cells) after 2 cycles of silica addition and drying (a–c, 30 ppm Si; d–f, 300 ppm Si). *30 ppm Si:* (**a**) General view of the deposit; note the distinction between granular silica material and smooth NaCl layers. (**b**) Close-up of a NaCl layer covering the silica precipitate; silica nanoparticles (tens of nanometers in size) appear present in topographic lows of the NaCl layer. (**c**) Sample rinsed with distilled water; NaCl is effectively removed, and only silica precipitates remain. *300 ppm Si:* (**d**) General view of the deposit; desiccation cracks have formed within the silica precipitate; NaCl crystals appear to have nucleated around cracks and boundaries of the silica deposit. (**e**) Side view of the deposit, showing two layers of different thickness within the silica precipitate; some individual NaCl crystals are visible on top of the deposit (arrow). (**f**) Close-up on a section of the deposit, showing the granular texture of the silica precipitate. All SEM micrographs were made at 5 kV on unrinsed samples, unless otherwise stated.

addition. No large, contiguous deposits of NaCl were observed, and instead, NaCl crystals appeared to form preferentially on cell surfaces (Fig. 3b), perhaps as a result of heterogeneous water distribution during the dessication process.

Experiments with 150 ppm Si solutions, which were rendered silica-oversaturated by pH adjustment immediately prior to use, generated significantly thicker deposits (Fig. 4a). After 10 cycles, almost all *S. elongatus* cells in the pellet were associated with authigenic silica precipitates (Fig. 4b, 4c). Instead of individual crystals, late-stage NaCl formed a uniform deposit on top of the silica mass, covering it almost entirely (Fig. 4a). At times, 30–70 nm nanoparticles of precipitated silica entirely filled void spaces between cells (Fig. 4b, 4c). Again, no distinct layering of silica could be seen resulting from sequential silica additions. All three forms of silica mineralization (granular mass, larger agglomerates, and fine coatings) observed in the 30 ppm Si experiments were again observed (Fig. 4b–d). As in the 30 ppm Si experiments, cells sometimes were covered with a layer of discrete silica particles that were finer than coexisting aggregates (25–55 nm vs. 30–70 nm; compare Figs. 3c and 4d), but also showed variations in the level of mineral precipitation (compare Fig. 4c and 4d). *S. elongatus* cells again appeared undamaged by the treatments (Fig. 4d).

In the case of experiments with 300 ppm Si oversaturated solutions, the total amount of silica precipitated after only 1 cycle is equivalent to 10 cycles with undersaturated 30 ppm Si solutions (Table 1). Despite this, the two samples looked significantly different (compare Figs. 3a and 5a). After complete evaporation, the cell-silica deposits appeared particularly flat, and *S. elongatus* cells were easily recognizable and trapped within an apparently bright matrix (Fig. 5a). Close-up micrographs show that the bright aspect of the matrix was due to small NaCl crystals that formed on its surface (Fig. 5b). These crystals were completely removed by rinsing, which unveiled the underlying smooth and homogeneous silica matrix comprising densely packed 20–40 nm silica

Table 1. Concentrations and Precipitated Mass of the Different Chemical Species Present in the Silica Solution

	Experiment Si concentration (ppm Si)		
	30	*150*	*300*
Percent solution evaporated when SiO_2 precipitation begins (**1**)	39	0 (initially oversaturated)	0 (initially oversaturated)
Initial silica solution saturation state ($\log(Q/K)$) (**2**)	−0.21	0.48	0.79
Mass of SiO_2 added per cycle (mg) (**3**)	0.064	0.321	0.642
Total mass of SiO_2 added over 10 cycles (mg)	0.642	3.209	6.418
Silica deposition rate ($kg \cdot yr^{-1} \cdot m^{-2}$) (**4**)	18.26	91.30	182.59
Initial [Na^+] (mmol/L) (**3**)	2.136	10.680	21.360
Initial [Cl^-] (mmol/L) (**5**)	1.704	10.080	20.160
Potential mass of NaCl added per cycle (mg) (**6**)	0.100	0.589	1.178
Salinity after 1 cycle (‰)	0.1	0.6	1.2
Potential total mass of NaCl formed over 10 cycles (mg)	0.996	5.891	11.782
Salinity after 10 cycles (‰)	1.0	5.9	11.8
Percent solution evaporated when NaCl precipitation begins (first cycle) (**7**)	99.97	99.84	99.67
Percent solution evaporated when NaCl precipitation begins (tenth cycle) (**7**)	99.72	98.36	96.72

(**1**) Silica solubility: 49 ppm Si at 20°C (from the equilibrium equation of Gunnarsson and Arnórsson, 2000).
(**2**) $\log(Q) = \log([H_4SiO_4])$; $\log(K) = -8.476 - 485.24 \times T^{-1} - 2.268 \times 10^{-6} \times T^2 + 3.068 \times \log(T)$ (Gunnarsson and Arnórsson, 2000), with $T = 293$ K.
(**3**) 1 mL of silica solution added per cycle. 300 ppm Si solution prepared by dissolving 0.304 g of $Na_2SiO_3 \cdot 9H_2O$ in 100 mL.
(**4**) 1 cycle = 1.5 day, surface of the polystyrene dish = 8.55×10^{-4} m^2.
(**5**) Calculated from the quantities of HCl necessary to obtain pH ~8.
(**6**) Calculated from initial [Cl^-] (which is lower than initial [Na^+]).
(**7**) NaCl solubility: 358.9 g/L at 20°C (Chase *et al.*, 1985).

particles (Fig. 5c). *S. elongatus* cells appeared mainly molded and trapped by silica (Fig. 5b, 5c), but a few smaller particles (15–30 nm) had nucleated on *S. elongatus* cell surfaces (Fig. 5c).

In experiments comprising 10 cycles with highly oversaturated 300 ppm Si solution, the resulting deposits were between 5 and 10 μm thick and consisted of two distinct layers: a homogeneous upper NaCl layer constituting approximately one-third of the total thickness, and a bottom 3–6 μm layer hosting a mixture of cells and granular silica precipitates consisting of an amalgamation of 25–50 nm particles (Fig. 6a, 6b). The limit between the two layers was well defined (Fig. 6b), and no traces of NaCl or other salts were evident in the lower silica mass. Once again, NaCl formed at the surface after each drying episode but was dissolved entirely during the next solution addition. The result appears to have been progressive deposition of silica, eventually forming a single silica deposit, upon which a NaCl layer was presumably repeatedly deposited and dissolved. Unlike the other cell pellet experiments, but comparable to the 300 ppm Si inorganic control, stratification within the silica deposit itself is visible but more difficult to discern due to the presence of cells (Fig. 6b). During the first 5–7 cycles, it appears that the deposition of silica progressively trapped cells, and complete entombment of the cell pellet was achieved. Layers of silica that formed afterward apparently only covered the previous deposit and formed quite uniform layers (*e.g.,* Fig. 6b, 6d). The deepest, initial silica layers appear denser than silica layers nearest to the surface (Fig. 6b). Compaction is an unlikely explanation; instead, percolation of silica solution and void infilling may have occurred during later additions. No differences in the size of the silica particles of the different layers could be seen. *S. elongatus* cells remain intact and continue to show no sign of degradation that might be expected from silica entombment or multiple drying/rehydration cycles (*e.g.,* Fig. 6c, 6e).

In addition to removing the NaCl layer, rinsing prior to SEM observation at times removed cells and revealed cell imprint casts in the fine granular silica matrix (Fig. 6e, 6f). These casts have sizes that are identical to the original cells, indicating that on the timescale of these experiments, cell silicification provides an accurate molding of the cells with no size or shape changes despite desiccation and repetitive additions of silica. Simulated diagenesis experiments have indicated that this is not always the case (Orange *et al.,* 2013). Silica mineralization of the cell was significantly lower than that of the 30 and 150 ppm Si experiments (compare Figs. 3c, 4d, and 6c), but 20–40 nm particles could be seen heterogeneously covering *S. elongatus* cells (Fig. 6c, 6f), indicating that successive silica additions did not lead to a significant increase in the size of the particles.

4. Discussion

4.1. Formation and microstructure of experimental sinters

In experiments without cells (Fig. 2), the repeated addition and evaporation of silica solutions, both over- and undersaturated with respect to amorphous silica, led to the formation of laminated deposits with silica layers corresponding to each evaporation cycle and with variable amounts of late-stage NaCl salts (Fig. 2b, 2e). Apart from obvious differences in the amount of silica precipitated, the structure of the deposit was similar for all concentrations. Higher (oversaturated) silica concentrations only led to a more dense silica deposit, but they did not appear to influence the size of the granular silica precipitate (30–40 nm). During evaporation, amorphous silica always precipitated first, even when the solution was initially undersaturated. NaCl only became supersaturated after >99% evaporation for the first cycle, or >96% after 10 cycles (Table 1), excluding any significant period of coprecipitation with silica.

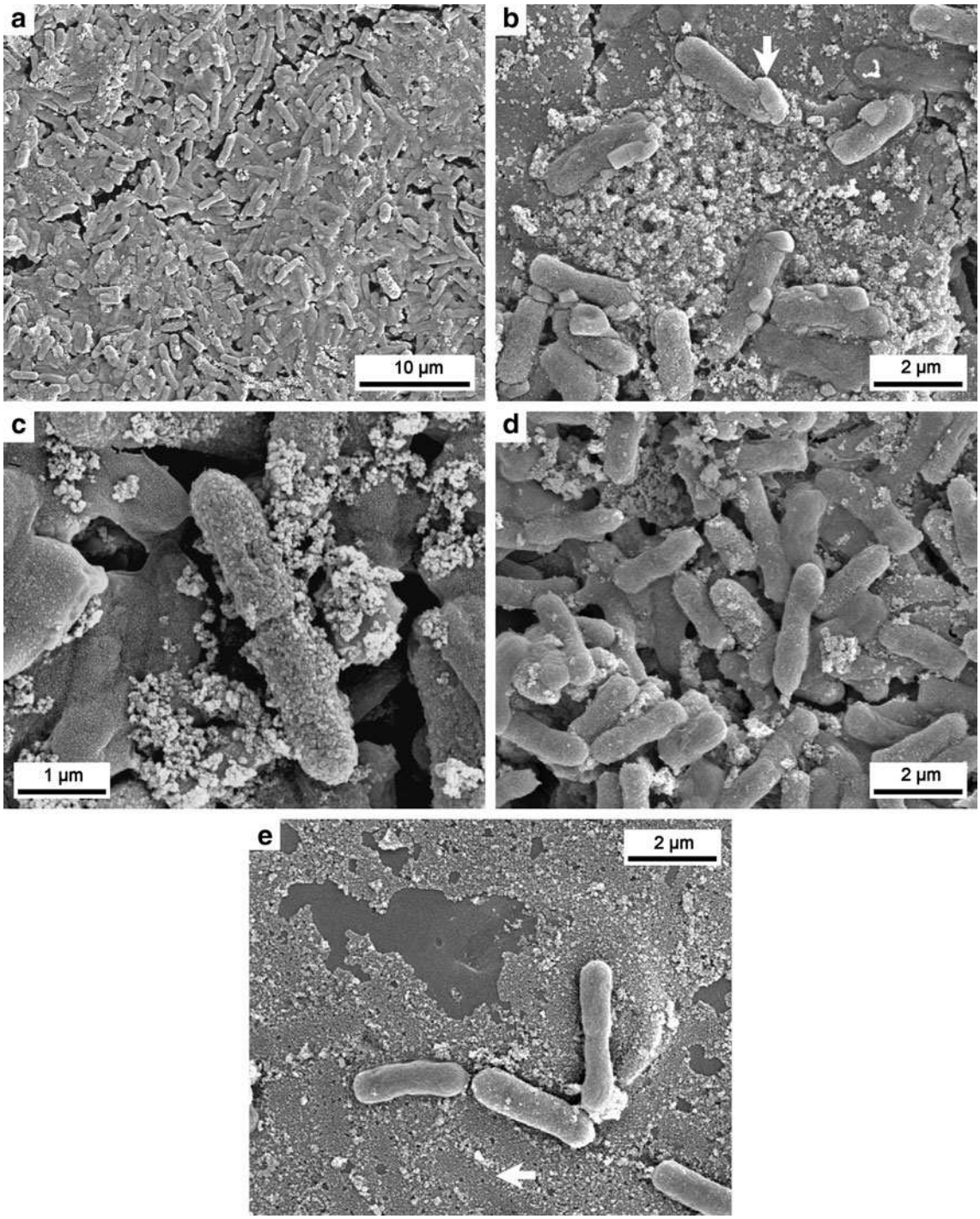

FIG. 3. SEM micrographs of a mineralized cell pellet of *Synechococus elongatus* after 10 cycles of silica addition/drying of a 30 ppm Si solution. (**a**) General aspect of the deposit; high cell density in all experiments resulted in dense masses of cells which appear covered and loosely connected by an EPS matrix. (**b**) *S. elongatus* cells and smooth EPS with silica aggregates on their surfaces; crystals of NaCl (arrow) appear uniquely associated with *S. elongatus* cells. (**c**) Mineralized and unmineralized *S. elongatus* cells in EPS matrix with silica nanoparticle aggregates. (**d**) Sample rinsed with distilled water; *S. elongatus* cells coated with EPS, showing various states of silicification and particle aggregation. (**e**) Sample rinsed with distilled water; the silica deposit formed directly on the polystyrene dish and on the edge of the cell layer; imprints of removed cells can be seen as outlined in silica particle aggregates (arrow); a wide range in silica particle sizes, from a fine-grained matrix to large particle aggregates, is apparent. All SEM micrographs were made at 5 kV on unrinsed samples, unless otherwise stated.

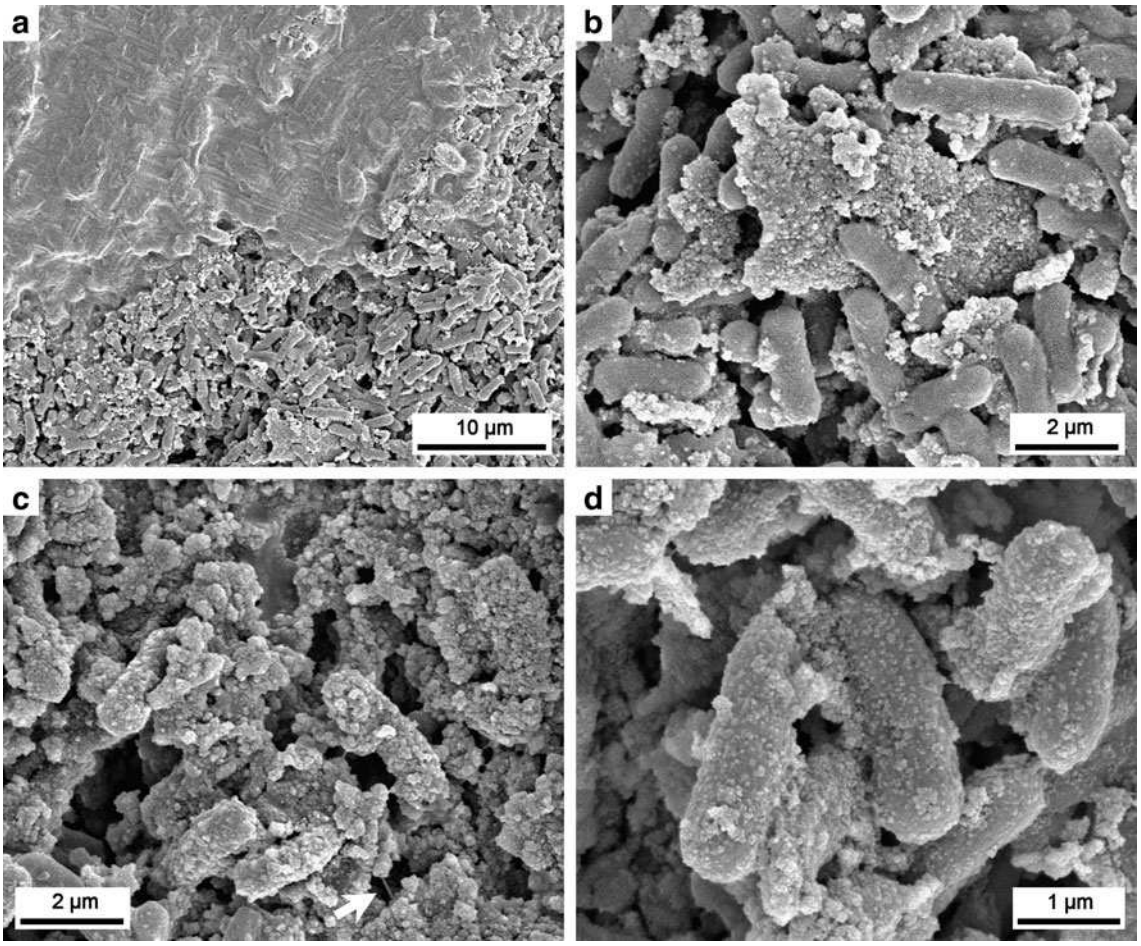

FIG. 4. SEM micrographs of a mineralized cell pellet of *Synechococus elongatus* after 10 cycles of silica addition/drying of a 150 ppm Si solution. (**a**) General aspect of the deposit; note the smooth NaCl precipitate partially covering the mineralized cell mass. (**b**) Aggregates of silica particles formed between *S. elongatus* cells. (**c**) Heavily mineralized *S. elongatus* cells; EPS filaments are visible (arrow). (**d**) Sample rinsed with distilled water; *S. elongatus* cells showing an intermediate mineralization relative to (b) and (c). All SEM micrographs were made at 5 kV on unrinsed samples, unless otherwise stated.

The addition of fresh silica solution apparently dissolved in its entirety any residual salts from the previous cycle (Fig. 2f). Despite sometimes reaching relatively high salinity values after 10 cycles (Table 1), we assumed that the dissolved NaCl did not have an influence on the size of the particles formed or the silica solubility, in accordance with the findings of Tobler *et al.* (2009). In the case of the most silica-supersaturated (300 ppm Si) inorganic experiment, two subsequent addition-evaporation cycles resulted in two distinct deposit layers of significantly different thickness, whereby the second cycle led to a thinner layer (Fig. 2f). The most likely explanation is that, during the second cycle, silica precipitated at first within void spaces of the previous silica layer. This is consistent with natural examples where sinters have been observed to be more or completely cemented at depth, for example, from rim to spicule core (Jones and Renaut, 2006) and top to bottom (Campbell *et al.*, 2001).

Silicification of cell biomass can occur from either particles preformed in suspension by homogeneous nucleation or by heterogeneous nucleation on cellular or inorganic surfaces. In both cases, a state of supersaturation is required for mineral formation (see review in Konhauser *et al.*, 2004). In our experiments that consisted of successive additions of silica, it is likely that both processes occurred in tandem. First, deposition of particles that formed in suspension during any one given cycle would result in the accumulation of particles of similar sizes but with perhaps the amount of silica particles that formed increasing in number with higher states of initial silica concentrations (*i.e.*, a nucleation-controlled regime where new surface area is created mainly by the nucleation of many small grains characterized by high surface-area-to-mass ratios; Steefel and Van Cappellen, 1990). Some of these particles would sediment onto cell biomass, while many would not end up associated with biomass. Simultaneously, silica nucleation also occurred on the cellular (wall, EPS) or inorganic surfaces. These initial crystals would be small in size but then grow after continued exposure to other silica additions (*i.e.*, crystal-growth regime). This is indeed what was observed in the 30 ppm Si and 150 ppm Si experiments, where particles grew from 30–40 nm after 2 cycles (Fig. 2b, 2c) to 30–70 nm after 10 cycles (Figs. 3c, 4b). Interestingly, in the 300 ppm Si experiments, the size of the particles of the silica matrix did not change significantly and remained around 20–40 nm even after repeated cycles (compare Figs. 5c and 6f). Moreover, the

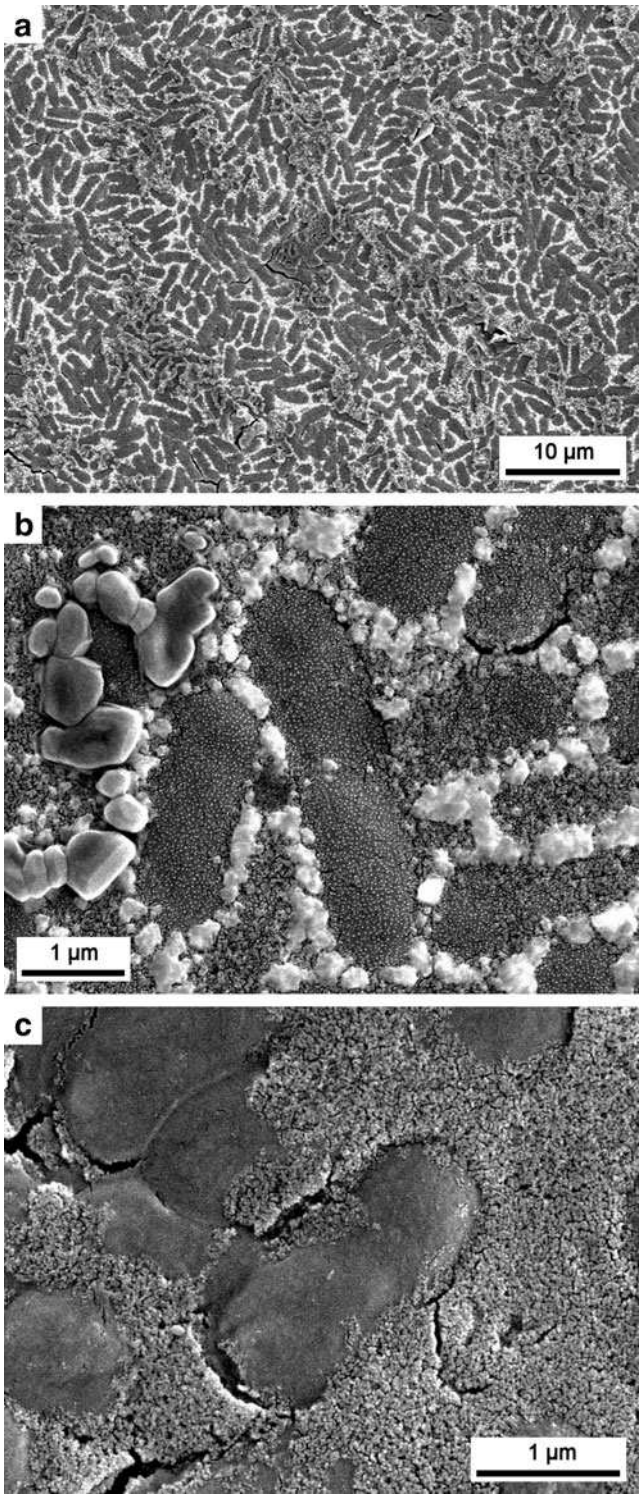

FIG. 5. SEM micrographs of a mineralized cell pellet of *Synechococus elongatus* after 1 cycle of silica addition/drying of a 300 ppm Si solution. (**a**) General aspect of the deposit; note the brightness of the silica matrix embedding the *S. elongatus* cells. (**b**) Close-up of the deposit; note the small NaCl crystals formed on top of the matrix and concentrated at cell boundaries. (**c**) Sample rinsed with distilled water; *S. elongatus* cells trapped in the granular silica matrix. All SEM micrographs were made at 5 kV on unrinsed samples, unless otherwise stated.

amount of silica particles bound to the cell surfaces was significantly lower in the 300 ppm Si experiment than that which occurred in the 30 and 150 ppm Si experiments (compare Figs. 4d and 6f), with most of the silica particles unassociated with *S. elongatus* cells. This difference supports the fact that silica precipitation occurred mainly by heterogeneous nucleation and growth on cellular and inorganic surfaces in the 30 and 150 ppm Si experiments and by homogeneous nucleation and deposition of preformed silica particles in the 300 ppm Si experiment. These collective observations highlight the classic division between nucleation-dominated regimes at high supersaturation and growth-dominated regimes at low supersaturation. Indeed, the greater overall size range of the particles at lower Si concentrations may be attributed in part to Ostwald ripening, a process in which—at lower degrees of saturation (growth-dominated or equilibrium regimes)—larger particles continue to grow at the expense of smaller particles that dissolve despite solution saturation (see Boistelle and Astier, 1988, for review). These observations also correlate well with previous studies that have argued that silicification at hot spring systems, where silica concentrations do not typically reach 300 ppm Si, is enhanced by the presence of reactive cell surfaces (Phoenix *et al.,* 2003; Yee *et al.,* 2003; Benning *et al.,* 2004a, 2004b; Konhauser *et al.,* 2004; Lalonde *et al.,* 2005, 2008a, 2008b), while deposition of preformed particles would be nonpreferential.

It is also worth noting that the presence of a layer of *S. elongatus* cells generally inhibited the formation of a laminated silica precipitate, relative to the experiments without cells. In particular, the 30 ppm Si and 150 ppm Si experiments did not result in the formation of well-defined silica layers, as most of the silica had precipitated on the cells or on the EPS mucus that binds them (Figs. 3b, 4c). Some thick silica deposits were seen from time to time for both silica concentrations (Figs. 3c, 4b) but were scarce in the 30 ppm Si experiment and insufficient to fill entirely the void space between cells in the 150 ppm Si experiment (Fig. 4c). In the 300 ppm Si experiment, silica not only filled this void space entirely (Fig. 6e) but also eventually completely entombed and covered the cells (Fig. 6d). Subsequent silica additions led to the formation of well-defined silica layers, similar to the experiment without cells, with uniform laminations and a progressive filling of one layer's porosity by silica coming from subsequent additions (Fig. 6b). Deposits that formed after successive cycles with 30, 150, or 300 ppm Si silica solution additions each reveal different stages or degrees of silicification, with a progression of silicification that depends on the concentrations added: at first precipitating directly on cells, then filling of voids between cells and eventual entombment.

A comparison of experiments with different initial silica solution concentrations but with the same total amount of silica added (*e.g.,* 10 cycles with 30 ppm Si solution vs. 1 with 300 ppm Si solution) reveals that initial concentration also plays a role in the sinter structure and formation. With the same amount of silica, 10 additions of a 30 ppm Si silica solution only resulted in a small and heterogeneous precipitation of silica on *S. elongatus* cells and rare silica aggregates (Fig. 3c). By contrast, one addition of a 300 ppm Si solution entirely filled the void space between cells (Fig. 5b, 5c) but with no significant mineralization of the cells. Similar to the

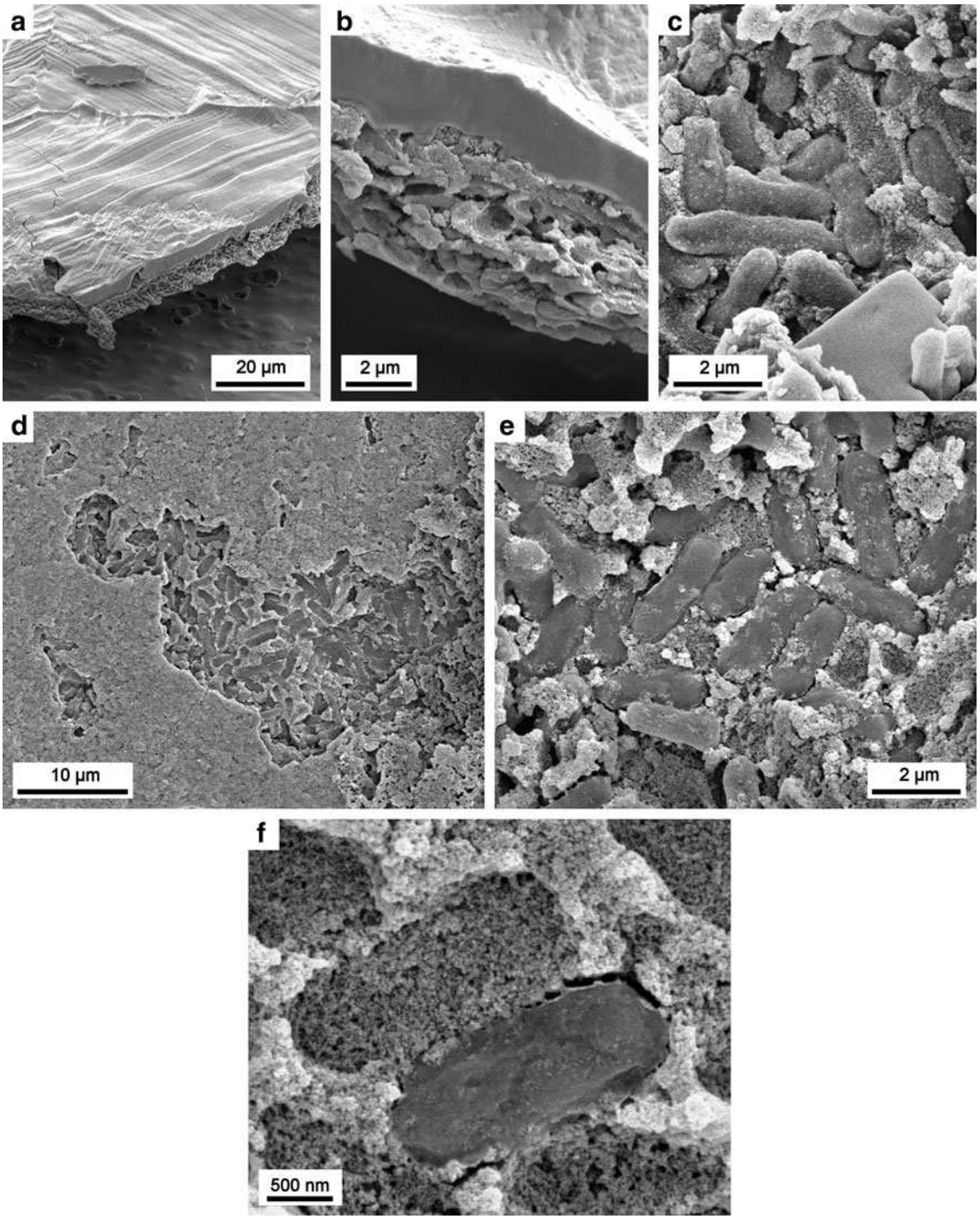

FIG. 6. SEM micrographs of a mineralized cell pellet of *Synechococus elongatus* after 10 cycles of silica addition and drying of a 300 ppm Si solution. (**a**) Side view of the deposit. (**b**) Close-up side view of the deposit showing a surface NaCl layer and a bottom, layered silica deposit encasing the *S. elongatus* cells. (**c**) *S. elongatus* cells trapped within the silica precipitate. (**d**) Sample rinsed with distilled water; top view showing trapped cells with a covering mass of silica. (**e**) Sample rinsed with distilled water; mineralized *S. elongatus* cells appear encased by silica but not extensively altered by it. (**f**) Sample rinsed with distilled water; trapped *S. elongatus* cell next to void cell casts in the silica matrix. All SEM micrographs were made at 5 kV on unrinsed samples, unless otherwise stated.

monitoring of the evolution of particle sizes, this suggests that in the 300 ppm Si experiment the high degree of oversaturation favored homogeneous nucleation and massive deposition as opposed to heterogeneous nucleation directly on the cell surfaces at 30 and 150 ppm Si.

4.2. Comparison with natural silica sinters

The experimental sinters described herein demonstrate several important commonalities with their natural counterparts, specifically their fabrics, cell mineralization, and

microstructure. First, despite tightly controlled conditions, the experimental sinters displayed significant fabric heterogeneity, with styles of mineralization ranging from cell-surface attachment of sparse colloids and aggregates (Fig. 3c, 3d) to complete cell coverage (*e.g.,* Fig. 4c, 4d) and eventually the complete encasement of the cells in a fine-grained mass of amorphous silica (*e.g.,* Figs. 5, 6d, 6f). Similar degrees of heterogeneity are widely reported in natural sinters. For example, within the well-preserved late-Pleistocene Umuriki sinter (Taupo Volcanic Zone, New Zealand), Campbell *et al.* (2001) identified three general silica fabrics. They included (i) a fine-grained porous and friable fabric, (ii) a dense vitreous fabric, and (iii) a more crystalline fabric. All three fabrics were presumed original to early diagenesis and appear broadly equivalent to the mineralization styles observed in our experiment (Figs. 4c and 6d). The third fabric observed by Campbell *et al.* (2001) is more crystalline and represents later stage diagenesis; such diagenesis was precluded by our experiments and, accordingly, no such fabric was observed.

Second, cells completely encrusted in a fine-grained mass of amorphous silica appeared well preserved and without evidence for significant degradation (*i.e.,* cell wall defect, dehydration, or collapse) (Figs. 3c, 4d, 6c). Due to the short duration of our experiment, however, it is difficult to estimate the effects of successive silica deposition and evaporation cycles on the long-term preservation of cells. Nonetheless, the different silicification patterns observed were similar to those that have been described from natural microfossils. The progressive covering of *S. elongatus* cells by the nucleation of fine-grained particles of silica on their walls, observed in the 30 and 150 ppm Si experiments (Figs. 3c, 4c), has previously been observed in numerous fossilization studies, performed *in situ* (Schultze-Lam *et al.,* 1995; Cady and Farmer, 1996; Konhauser *et al.,* 2001; Jones *et al.,* 1998, 2001, 2003, 2004; Handley *et al.,* 2005; Tobler *et al.,* 2008) and *in vitro* (Oehler and Schopf, 1971; Oehler, 1976; Ferris *et al.,* 1988; Birnbaum *et al.,* 1989; Westall *et al.,* 1995; Westall, 1997; Toporski *et al.,* 2002; Lalonde *et al.,* 2005; Orange *et al.,* 2009, 2011). The complete entombment of the cells in a dense silica matrix observed in the 300 ppm Si experiment (Fig. 6d), and the formation of molds preserving the morphology of the cells (Fig. 6f), has also been widely described during the formation of silica sinters (Cady and Farmer, 1996; Jones *et al.,* 1998, 2001, 2003, 2005; Kyle *et al.,* 2007; Tobler *et al.,* 2008; Parenteau and Cady, 2010). The absence of changes in the size and shape of these molds, despite repeated cycles of desiccation and silica addition, illustrates that dense silica deposits that form as a result of evaporation may be particularly resistant to mechanical deformation, as previously noted by Hinman and Lindstrom (1996) and Orange *et al.* (2013).

Third, structural analogies of the simulated sinter with their natural counterparts are limited to their microstructure. As previously mentioned, and as noted in our experimental simulations, the sinter microstructure can easily be influenced by the presence of microorganisms. In the absence of microorganisms (in the control experiments or in the 300 ppm Si experiment after complete entombment of the cells; Figs. 2a, 2f, 6b), the thin and regular micrometric laminae observed are similar to those reported for geyserites that form in proximity to alkaline hot springs where high temperatures prevent the development of microbial mats (Walter 1972, 1976a). Under such circumstances, lamination derives from the intermittent supply of silica (*e.g.,* through splash during spring surges or geyser eruptions). In areas densely populated by microorganisms, micrometer-scale laminae are generally absent, and thicker laminated structures (tens to hundreds of micrometers thick) form as the result of daily or seasonal variations in microbial activity. Such is the case for many hot spring stromatolites, where lamination arises from an alternation of microbially mediated porous laminae and abiotically formed laminae, or an alternation between horizontally and vertically orientated silicified filamentous microorganisms (Walter, 1972; Walter *et al.,* 1976; Hinman and Lindstrom, 1996, Jones *et al.,* 1998, 2005; Konhauser *et al.,* 2001; Handley *et al.,* 2005; Berelson *et al.,* 2011). The cell pellets used in our study were not an actively growing microbial community. Therefore, this prevented us from observing sinter structures such as laminae that form as a result of temporal variations in microbial growth (Berelson *et al.,* 2011) or spicules that are usually found in hot spring pool inner rims and form by using microcolonies as templates (Handley *et al.,* 2005; Schinteie *et al.,* 2007).

With that said, by acting as a surface for heterogeneous nucleation of silica particles, *S. elongatus* cells proved to be influential on the deposition of silica and the fabrics of the sinter despite the short timescales of our experiments. For instance, the thick silica deposit that formed progressively in the 300 ppm Si experiment (Fig. 6b) included a heterogeneous layer that was strongly influenced by the presence of microorganisms and a more homogeneous layer that formed after complete entombment of microorganisms, thus bearing analogies with the natural laminated microstromatolites. In all cases (abiotic or microbially influenced sinter formation), the macrostructure is determined by environmental factors such as the location of the sinter with respect to the spring (pool, outer and inner rim, discharge apron, outflow channel), the spring style and activity (*i.e.,* quiet, surging, boiling, geyser; Braunstein and Lowe, 2001), or other parameters (*i.e.,* silica concentration, air temperature; Hinman and Lindstrom, 1996). All these factors have not been simulated in our experiments. Limitations in size and duration prevented us from observing the development of macrostructural features such as terraced, digitate, or columnar sinters (Jones *et al.,* 1998; Braunstein and Lowe, 2001). A longer study, with a prolonged supply of dissolved silica, might possibly have led to the formation of such structures, as was the case in sinter growth studies performed *in situ* on glass substrates (Mountain *et al.,* 2003; Handley *et al.,* 2005; Tobler *et al.,* 2008).

Finally, special consideration of natural and experimental silica deposition rates is warranted to better understand the applicability of experimentally generated silica sinter and silica biomineralization experiments in general to the context of natural settings. This work constitutes, to our knowledge, the first experimental study with the aim of ascertaining the importance of evaporative processes on the formation of some natural sinters (Jones *et al.,* 1998; Braunstein and Lowe, 2001; Mountain *et al.,* 2003; Handley *et al.,* 2005; Schinteie *et al.,* 2007; Tobler *et al.,* 2008). Importantly, the relationship between the initial degree of silica supersaturation of a solution and its potential for silica deposition is significantly different between the scenarios of complete evaporation and

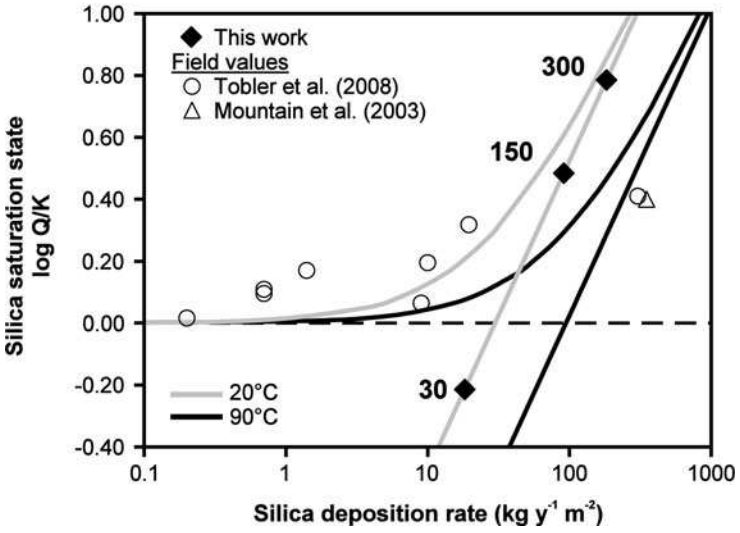

FIG. 7. Calculated silica deposition rates for equilibrium precipitation from supersaturated solutions (curved lines) and after complete evaporation (straight lines) as calculated for two temperatures (20°C, gray lines; 90°C, black lines). Data points represent natural examples where sinter deposition rates were published (circles and triangle; Mountain *et al.*, 2003; Tobler *et al.*, 2008) and the experimental sinters described herein (30, 150, 300 ppm Si experiments, black diamonds). See text for further explanation.

simple re-equilibration of a saturated solution. Complete evaporation of a silica-bearing solution will lead to silica deposition regardless of initial saturation state, whereas for a solution that is simply re-equilibrating, deposition approaches zero as its initial composition approaches saturation. This relationship is demonstrated in Fig. 7, where silica deposition rates [in $kg(SiO_2)\cdot yr^{-1}\cdot m^{-2}$] are plotted as a function of initial solution saturation state [expressed as $\log(Q/K)$]. Q is the ion product of the equation $SiO_2 + 2\,H_2O \rightleftarrows H_4SiO$ and is equal to $[H_4SiO_4]$, and K is the solubility product, calculated from the equilibrium equation of Gunnarsson and Arnórsson (2000): $\log(K) = -8.476 - 485.24\times T^{-1} - 2.268\times10^{-6}\times T^2 + 3.068\times\log(T)$. Model lines corresponding to silica deposition after either complete evaporation (straight lines) or chemical equilibrium silica deposition (curved lines) are drawn by using the aforementioned equilibrium equation for calculating $\log(Q/K)$ and silica solubility at 20°C and 90°C and by using the parameters of our sinter growth experiments for calculating silica deposition rates for different initial silica concentrations in both cases of complete evaporation and chemical equilibrium. In highly silica-supersatured solutions, the precipitation of silica as the result of equilibration approaches the case of complete evaporation (upper right portion of the plot) as a greater proportion of the total silica is deposited. Also plotted are sinter growth rates and silica saturation parameters collected from field studies in New Zealand and Iceland (Mountain *et al.*, 2003; Tobler *et al.*, 2008). This representation puts into perspective the relationships between saturation state and silica deposition rate for both natural and experimental sinters. Experimental deposition rates were within the range observed for natural systems, and they span their saturation states. The lowest Si concentration experiment (30 ppm Si) is the only one that was initially silica-undersaturated and thus fell in the evaporation-only field (deposition below initial $\log Q/K = 0$). Natural systems with low deposition rates appear consistent with precipitation after physicochemical equilibrium, falling along curved lines (chemical equilibrium precipitation models). The deposition rates observed in the 150 and 300 ppm Si experiments, being close to physicochemical equilibrium line, appear to follow the trend of these natural systems. The most rapidly depositing natural sinters [$>300\,kg(SiO_2)\cdot yr^{-1}\cdot m^{-2}$] fall to the right of model lines, indicating anomalously fast precipitation; this may be due to additional parameters (notably cooling) that were not considered (*cf.* difference between 20°C and 90°C model lines).

In addition, the thickness of the sinter obtained at the end of the 300 ppm Si experiment (3–6 μm) would translate into an annual growth of $\sim$0.1 mm/yr. This value is lower than the value measured in natural sinters, such as 0.2–0.9 mm/yr at Champagne Pool, New Zealand (Jones *et al.*, 1999); 0.45–0.9 mm/yr at Krisuvik hot spring, Iceland (Konhauser *et al.*, 2001); 0.5–1.0 mm/yr at Yellowstone National Park, USA (Braunstein and Lowe, 2001); $\sim$1 mm/yr at Warakei, New Zealand (Smyth *et al.*, 2003); $<$1 mm/yr to 24 mm/yr at various Yellowstone hot springs (Hinman and Lindstrom, 1996); and 10–50 mm/yr at Obsidian Pool Prime, Yellowstone, USA (Berelson *et al.*, 2011). The differences in deposition rates between our experiments and natural sinters is not surprising and may be explained by several factors. First, our experiments represent discrete simulations (*e.g.*, 10×36 h cycles) of natural sinter growth that may be continuous or punctuated in nature (*e.g.*, Berelson *et al.*, 2011). They thus lack the variability and complexity of environmental conditions, particularly as relating to silica input during subaerial sinter growth (*e.g.*, waves, splashes; capillary action; Hinman and Lindstrom, 1996; Mountain *et al.*, 2003; Handley *et al.*, 2005), pH changes (solubility calculations of Fig. 7 are only valid for pH <9 where $H_4SiO_4^\circ >> H_3SiO_4^-$), and temperature (all experiments in the current study were performed at room temperature). Second, our experiments also did not involve the continuous flow of silica-saturated waters above the sinter surface for a 1 yr period, with which to better compare our results to natural hot springs. Nonetheless, the consideration of precipitation rates as in Fig. 7 represents a first step toward better calibrating or evaluating experimental silicification studies in the context of their natural counterparts.

5. Conclusion

Despite limitations in time and space, this study has successfully recreated and examined some of the basic processes relating to silica sinter formation in a hot spring system as a result of evaporation and under the influence of a common

sinter-containing cyanobacterium. In the absence of microorganisms, successive addition and evaporation of silica solutions led to the formation of laminated deposits made of fine-grained silica particles, irrespective of the initial silica concentration used. Subsequent cycles of silica addition infilled the void spaces of previously deposited layers, thus resulting in a denser matrix. By contrast, the presence of *S. elongatus* cells greatly disturbed the formation of laminated deposits. Sinters with different structures were obtained depending on the initial silica concentration. For undersaturated and moderately oversaturated solutions (30 and 150 ppm Si, respectively), silica precipitated mainly on *S. elongatus* cell walls and EPS, resulting in a disorganized and porous sinter. Cells were efficiently silicified and progressively covered by silica particles. For the most oversaturated experimental condition (300 ppm Si), the resulting sinter matrix was dense, with silica infilling the void spaces between cells and resulting in their complete entombment despite limited direct cell surface silicification. Importantly, not only were these differences related to differences in the amount of silica added between each experiment, but they were also due to accompanying differences in the mechanisms of silica precipitation. In undersaturated and moderately oversaturated solutions, silica seemed to have precipitated mainly by heterogeneous nucleation on available surfaces (cell surface, silica particles), while in the highly oversaturated silica solution, deposition of silica particles that were preformed in suspension was favored. The sinters obtained through these simple experiments show numerous similarities with their natural counterparts, especially regarding their fabrics, microstructure, extent of microbial silicification, and silica deposition rate. These experiments enhance our understanding for silica sinter development and thus represent an important complement for *in situ* sinter growth studies. They also set the stage for subsequent experiments designed to examine a wider range of environmental conditions or longer episodes of silicification.

Acknowledgments

The authors thank Dr. George W. Owttrim and Dana Chamot (Department of Biological Sciences, University of Alberta) for providing the cyanobacteria fresh cultures, DeAnn Rollings and George Braybrook (Scanning Electron Microscope Laboratory, Department of Earth and Atmospheric Sciences, University of Alberta) for their help with the SEM, and the two anonymous reviewers for their helpful comments on this manuscript. F.O. was funded by the European Science Foundation ArchEnviron Exchange Grant #2723, and S.V.L. and K.O.K by the Natural Sciences and Engineering Research Council of Canada.

Abbreviations

EPS, extracellular polymeric substance; SEM, scanning electron microscope.

References

Benning, L.G., Phoenix, V.R., Yee, N., and Tobin, M.J. (2004a) Molecular characterization of cyanobacterial silicification using synchrotron infrared micro-spectroscopy. *Geochim Cosmochim Acta* 68:729–741.

Benning, L.G., Phoenix, V.R., Yee, N., and Konhauser, K.O. (2004b) The dynamics of cyanobacterial silicification: an infrared micro-spectroscopic investigation. *Geochim Cosmochim Acta* 68:743–757.

Berelson, W.M., Corsetti, F.A., Pepe-Ranney, C., Hammond, D.E., Beaumont, W., and Spear, J.R. (2011) Hot spring siliceous stromatolites from Yellowstone National Park: assessing growth rate and laminae formation. *Geobiology* 9:411–424.

Birnbaum, S.J., Wireman, J.W., and Borowski, R. (1989) Silica precipitation by the anaerobic sulphate reducing bacterium *Desulfovibrio desulfuricans:* effects upon cell morphology and implications for preservation. In *Origin, Evolution, and Modern Aspects of Biomineralization in Plants and Animals*, edited by R.E. Crick, Plenum Press, New York, pp 507–516.

Boistelle, R. and Astier, J.P. (1988) Crystallization mechanisms in solution. *J Cryst Growth* 90:14–30.

Braunstein, D. and Lowe, D.R. (2001) Relationship between spring and geyser activity and the deposition and morphology of high temperature (>73°C) siliceous sinter, Yellowstone National Park, Wyoming, USA. *Journal of Sedimentary Research* 71:747–763.

Cady, S.L. and Farmer, J.D. (1996) Fossilization processes in siliceous thermal springs: trends in preservation along thermal gradients. In *Evolution of Hydrothermal Ecosystems on Earth (and Mars?)*, edited by G.R. Bock and J.A. Goode, John Wiley and Sons, New York, pp 150–173.

Campbell, K.A, Sannazzaro, K., Rodgers, K.A., Herdinaita, N.R., and Browne, P.R.L. (2001) Sedimentary facies and mineralogy of the late Pleistocene Umukuri silica sinter, Taupo Volcanic Zone, New Zealand. *Journal of Sedimentary Research* 71: 727–746.

Chamot, D. and Owttrim, G.W. (2000) Regulation of cold shock-induced RNA helicase gene expression in the cyanobacterium *Anabaena* sp. strain PCC 7120. *J Bacteriol* 182: 1251–1256.

Chase, M.W., Davies, C.A., Downey, J.R., Frurip, D.J., McDonald, R.A., and Syverud, A.N. (1985) JANAF Thermochemical Tables, third edition. *Journal of Physical and Chemical Reference Data,* Supplement 14.

Chen, Y. (2007) Functional genomics of the unicellular cyanobacterium *Synechococcus elongatus* PCC 7942. PhD thesis, Division of Biological Sciences, Texas A&M University, College Station, TX.

Ferris, F.G., Fyfe, W.S., and Beveridge, T.J. (1988) Metallic ion binding by *Bacillus subtilis:* implications for the fossilization of microorganisms. *Geology* 16:149–152.

Ferris, M.J., Ruff-Roberts, A.L., Kopczynski, E.D., Bateson, M.M., and Ward, D.M. (1996) Enrichment culture and microscopy conceal diverse thermophilic *Synechococcus* populations in a single hot spring microbial mat habitat. *Appl Environ Microbiol* 62:1045–1050.

Fournier, R.O. (1985) The behavior of silica in hydrothermal solutions. In *Geology and Geochemistry of Epithermal Systems*, Reviews in Economic Geology, Vol. 2, edited by B.R. Berger and P.M. Bethke, Society of Economic Geologists, Littleton, CO, pp 45–61.

Gunnarsson, I. and Arnórsson, S. (2000) Amorphous silica solubility and the thermodynamics properties of $H_4SiO_4°$ in the range of 0° to 350°C at P_{sat}. *Geochim Cosmochim Acta* 64:2295–2307.

Handley, K.M., Campbell, K.A., Mountain, B.W., and Browne, P.R.L. (2005) Abiotic-biotic controls on the origin and development of spicular sinter: *in situ* growth experiments, Champagne Pool, Waiotapu, New Zealand. *Geobiology* 3:93–114.

Handley, K.M., Turner, S.J., Campbell, K.A., and Mountain, B.W. (2008) Silicifying biofilm exopolymers on a hot-spring microstromatolite: templating nanometer-thick laminae. *Astrobiology* 8:747–770.

Hinman, N.W. and Lindstrom, R.F. (1996) Seasonal changes in silica deposition in hot springs systems. *Chem Geol* 132:237–246.

Jones, B. and Renaut, R.W. (2006) Growth of siliceous spicules in acidic hot springs, Waiatapu geothermal area, North Island, New Zealand. *Palaios* 21:406–423.

Jones, B., Renaut, R.W., and Rosen, M.R. (1997) Biogenicity of silica precipitation around geysers and hot spring vents, North Island, New Zealand. *Journal of Sedimentary Research* 67:88–104.

Jones, B., Renaut, R.W., and Rosen, M.R. (1998) Microbial biofacies in hot-spring sinters: a model based on Ohaaki Pool, North Island, New Zealand. *Journal of Sedimentary Research* 68:413–434.

Jones, B., Renaut, R.W., and Rosen, M.R. (1999) Actively growing siliceous oncoids in the Waiotapu geothermal area, North Island, New Zealand. *J Geol Soc London* 156:89–103.

Jones, B., Renaut, R.W., and Rosen, M.R. (2000) Stromatolites forming in acidic hot-spring waters, North Island, New Zealand. *Palaios* 15:450–475.

Jones, B., Renaut, R.W., and Rosen, M.R. (2001) Taphonomy of silicified filamentous microbes—implications for identification. *Palaios* 16:580–592.

Jones, B., Renaut, R.W., and Rosen, M.R. (2003) Silicified microbes in a geyser mound: the enigma of low-temperature cyanobacteria in a high temperature setting. *Palaios* 18: 87–109.

Jones, B., Konhauser, K.O., Renaut, R.W., and Wheeler, R. (2004) Microbial silicification in Iodine Pool, Waimangu geothermal area, North Island, New Zealand: implications for recognition and identification of ancient silicified microbes. *J Geol Soc London* 161:983–993.

Jones, B., Renaut, R.W., and Konhauser, K.O. (2005) Genesis of large siliceous stromatolites at Frying Pan Lake, Waimangu geothermal field, North Island, New Zealand. *Sedimentology* 52:1229–1252.

Jones, B., de Ronde, C.E.J., and Renaut, R.W. (2008) Mineralized microbes from Giggenbach submarine volcano. *J Geophys Res* 113, doi:10.1029/2007JB005482.

Konhauser, K.O., Phoenix, V.R., Bottrell, S.H., Adams, D.G., and Head, I.M. (2001) Microbial–silica interactions in Icelandic hot spring sinter: possible analogues for some Precambrian siliceous stromatolites. *Sedimentology* 48:415–433.

Konhauser, K.O., Jones, B., Phoenix, V.R., Ferris, G., and Renaut, R.W. (2004) The microbial role in hot spring silicification. *Ambio* 33:552–558.

Kyle, J.E., Schroeder, P.A., and Wiegel, J. (2007) Microbial silicification in sinters from two terrestrial hot springs in the Uzon Caldera, Kamchatka, Russia. *Geomicrobiol J* 24:627–641.

Lalonde, S.V., Konhauser, K.O., Reysenbach, A.L., and Ferris, F.G. (2005) The experimental silicification of Aquificales and their role in hot spring formation. *Geobiology* 3:41–52.

Lalonde, S.V., Smith, D.S., Owttrim, G.W., and Konhauser, K.O. (2008a) Acid-base properties of cyanobacterial surfaces I: Influences of growth phase and nitrogen metabolism on surface reactivity. *Geochim Cosmochim Acta* 72:1257–1268.

Lalonde, S.V., Smith, D.S., Owttrim, G.W., and Konhauser, K.O. (2008b) Acid-base properties of cyanobacterial surfaces II: Silica as a chemical stressor influencing cell surface reactivity. *Geochim Cosmochim Acta* 72:1269–1280.

Mountain, B.W., Benning, L.G., and Boerema, J. (2003) Experimental studies on New Zealand hot spring sinters: rates of growth and textural development. *Can J Earth Sci* 40:1643–1667.

Oehler, J.H. (1976) Experimental studies in Precambrian paleontology: structural and chemical changes in blue-green algae during simulated fossilization in synthetic chert. *Geol Soc Am Bull* 87:117–129.

Oehler, J.H. and Schopf, J.W. (1971) Artificial microfossils: experimental studies of permineralization of blue-green algae in silica. *Science* 174:1229–1231.

Orange, F., Westall, F., Disnar, J.R., Prieur, D., Bienvenu, N., Le Romancer, M., and Défarge, C. (2009) Experimental silicification of the extremophilic archaea *Pyrococcus abyssi* and *Methanocaldococcus jannaschii*. Applications in the search for evidence of life in early Earth and extraterrestrial rocks. *Geobiology* 7:403–418.

Orange, F., Disnar, J.R., Westall, F., Prieur, D., and Baillif, P. (2011) Metal binding by the early Earth analogue microorganism, archaea *Methanocaldococcus jannaschii* and its effects on silicification. *Palaeontology* 54:953–964.

Orange, F., Lalonde, S.V., and Konhauser, K.O. (2013) The formation and preservation of *Synechococcus elongatus* cell moulds in simulated silica sinter: implications for the identification of microfossils. *Geomicrobiol J* doi:10.1080/01490451.2012.688926, in press.

Parenteau, M.N. and Cady, S.L. (2010) Microbial biosignatures in iron-mineralized phototrophic mats at Chocolate Pots hot springs, Yellowstone National Park, United States. *Palaios* 25:97–111.

Phoenix, V.R., Adams, D.G., and Konhauser, K.O. (2000) Cyanobacterial viability during hydrothermal biomineralization. *Chem Geol* 169:329–338.

Phoenix, V.R., Konhauser, K.O., and Ferris, F.G. (2003) Experimental study of iron and silica immobilization by bacteria in mixed Fe-Si systems: implications for microbial silicification in hot-springs. *Can J Earth Sci* 40:1669–1678.

Renaut, R.W., Jones, B., and Rosen, M.R. (1996) Primary silica oncoids from Orakeikorako hot springs, North Island, New Zealand. *Palaios* 11:446–458.

Rippka, R., Deruelles, J., Waterbury, J.B., Herdman, M., and Stanier, R.Y. (1979) Generic assignments, strain histories and properties of pure cultures of cyanobacteria. *J Gen Microbiol* 111:1–61.

Schinteie, R., Campbell, K.A., and Browne, P.R.L. (2007) Microfacies of stromatolitic sinter from acid-sulphate-chloride springs at Parariki Stream, Rotokawa geothermal field, New Zealand. *Palaeontol Electronica* 10:4A.

Schultze-Lam, S., Ferris, F.G., Konhauser, K.O., and Wiese, R.G. (1995) *In situ* silicification of an Icelandic microbial mat: implications for microfossil formation. *Can J Earth Sci* 32:2021–2026.

Smyth, B.Y., Turner, S.J., and Rodgers, K.A. (2003) Opal-A and associated microbes from Wairakei, New Zealand: the first 300 days. *Mineral Mag* 67:563–579.

Steefel, C.I. and Van Cappellen, P. (1990) A new kinetic approach to modeling water-rock interactions: the role of nucleation, precursors, and Ostwald ripening. *Geochim Cosmochim Acta* 54:2657–2677.

Tobler, D.J., Stefánsson, A., and Benning, L.G. (2008) *In-situ* grown silica sinters in Icelandic geothermal areas. *Geobiology* 6:481–502.

Tobler, D.J., Shaw, S., and Benning, L.G. (2009) Quantification of initial steps of nucleation and growth of silica nanoparticles: an *in-situ* SAXS and DLS study. *Geochim Cosmochim Acta* 73:5377–5393.

Toporski, J.K.W., Steele, A., Westall, F., Thomas-Keprta, K.L., and McKay, D.S. (2002) The simulated silicification of bacteria—new clues to the modes and timing of bacterial preservation and implications for the search for extraterrestrial microfossils. *Astrobiology* 2:1–26.

Walter, M.R. (1972) A hot spring analog for the depositional environment of Precambrian iron formations of the Lake Superior region. *Econ Geol* 67:965–980.

Walter, M.R. (1976a) Geyserites of Yellowstone National Park: an example of abiogenic "stromatolites". In *Stromatolites,* edited by M.R. Walter, Elsevier Scientific Publishing Company, Amsterdam, pp 87–112.

Walter, M.R. (1976b) Hot spring sediments in Yellowstone National Park. In *Stromatolites,* edited by M.R. Walter, Elsevier Scientific Publishing Company, Amsterdam, pp 489–498.

Walter, M.R., Bauld, J., and Brock, T.D. (1972) Siliceous algal and bacterial stromatolites in hot springs and geyser effluents of Yellowstone National Park. *Science* 178:402–405.

Walter, M.R., Bauld, J., and Brock, T.D. (1976) Microbiology and morphogenesis of columnar stromatolites (*Conophyton*, *Vacerrilla*) from hot springs in Yellowstone National Park. In *Stromatolites,* edited by M.R. Walter, Elsevier Scientific Publishing Company, Amsterdam, pp 273–310.

Westall, F. (1997) The influence of cell wall composition on the fossilization of bacteria and the implications for the search for early life forms. In *Astronomical and Biochemical Origins and the Search for Life in the Universe,* edited by C. Cosmovici, S. Bowyer, and D. Werthimer, Editori Compositrici, Bologna, pp 491–504.

Westall, F., Boni, L., and Guerzoni, E. (1995) The experimental silicification of microorganisms. *Paleontology* 38: 495–528.

White, D.E., Brannock, W.W., and Murata, K.J. (1956) Silica in hot-spring waters. *Geochim Cosmochim Acta* 10:27–59.

Yee, N., Phoenix, V.R., Konhauser, K.O., Benning, L.G., and Ferris, F.G. (2003) The effect of cyanobacteria on silica precipitation at neutral pH: implications for bacterial silicification in geothermal hot springs. *Chem Geol* 199:83–90.

Address correspondence to:
François Orange
University of Puerto Rico
Nanoscopy Facility
Facultad de Ciencias Naturales
Departamento de Fisica
PO Box 70377
San Juan PR 00936-8377
USA

E-mail: francois.orange@gmail.com

Submitted 12 June 2012
Accepted 7 November 2012